Stark broadening of satellite lines in silicon plasmas driven by femtosecond laser pulses

R. C. Mancini and A. S. Shlyaptseva
Department of Physics, University of Nevada, Reno, Nevada 89557-0058

P. Audebert, J. P. Geindre, S. Bastiani, and J. C. Gauthier
Laboratoire pour l'Utilisation des Lasers Intenses, Ecole Polytechnique, 91128 Palaiseau, France

G. Grillon, A. Mysyrowicz, and A. Antonetti
Laboratoire d'Optique Appliquée, Batterie de l'Yvette, 91120 Palaiseau, France
(Received 23 April 1996)

Silicon targets irradiated at large incidence angle (60°) with ultrashort (120 fs) *P*-polarized laser pulses at high intensities ($\approx 10^{16}$ W cm^{-2}) display significantly broadened *K*-shell x-ray line emission. To analyze the spectra we have calculated Stark-broadened line profiles for the He_α resonance line and its satellite transitions in Li-, Be-, and B-like ions with spectator electrons in the *L* and *M* shells. Results indicate that the emission is characteristic of near solid densities and that there is an unusually high contribution from high-order satellite transitions; this could be due to a combination of high-density and transient effects. [S1063-651X(96)00610-1]

PACS number(s): 52.50.Jm, 52.40.Nk, 32.30.Rj, 32.70.Jz

I. INTRODUCTION

The use of subpicosecond pulsed lasers to irradiate solid targets has opened a new area of research in laser-produced plasmas. The laser energy absorbed in a thin layer of material close to the surface produces a plasma whose lifetime is comparable to the duration of the laser pulse and whose spatial extension is of the order of the skin depth. These plasmas provide an excellent opportunity to observe high-density, and time-dependent and nonequilibrium effects in laser-produced plasmas. If the prepulse or pedestal of the main laser pulse is minimized (high contrast pulses) then the ultrashort, high-intensity pulse couples to the target, thus producing a plasma of near solid density that undergoes rapid heating and cooling and moderate hydrodynamic expansion; under these conditions the plasma can radiate a bright and ultrashort pulse of x rays [1–3].

X-ray spectroscopic measurements of the radiation emitted by these plasmas represent a useful diagnostic technique to help understand laser-target coupling, plasma atomic kinetics and x-ray emission, and transport of energy towards the bulk of the target [3–9]. In particular, line intensity and broadening measurements of aluminum He_γ, He_β, and Ly_α lines have been used to infer average electron density and temperature in experiments performed with 400-fs duration laser pulses [3,7]. Detailed spectroscopic analysis of Li-like satellite emission from aluminum targets irradiated with subpicosecond laser pulses (100-fs and 400-fs duration) has recently shown how nonequilibrium and transient atomic kinetics can affect the distribution of population of doubly excited states in Li-like ions and the signature that this produces in the spectral intensity distribution [10–12]. Also, x-ray spectroscopy of K_α line emission has been applied to the diagnosis of hot-electron production and transport [13–15], to the observation of $KL \rightarrow LL$ x-ray satellite emission [16], and in studies of plasma confinement by the ponderomotive force induced by the laser pulse [17].

In this paper we report on the observation and line broadening analysis of K_α x-ray emission from silicon targets irradiated with high-contrast, femtosecond laser pulses. The spectra show emissions from the cold K_α to the He_α. Here we will focus on the analysis of the spectral features associated with Be-, Li-, and He-like ions. An analysis of the full sequence of *L*-shell ions will be presented later.

The Li-like spectral feature is particularly interesting since it has been observed under a broad range of plasma conditions [18]: astrophysical environments, magnetic and laser fusion energy experiments, long-pulse laser-produced plasmas, and, more recently, in ultrashort-pulse laser-plasma experiments performed under conditions different from those reported here [10–12]. Accordingly, its intensity distribution and broadening properties [19] have been studied in the corona model, collisional-radiative equilibrium, local thermodynamic equilibrium (LTE) approximation, and transient cases.

Yet here we report on properties not observed before, as far as we know, namely, the broadening and blending with Be-like satellite transitions under high-density and transient conditions, where the Be emission becomes comparable and even more intense than the Li emission. This blending changes the intensity distribution and overall broadening of the Li spectral feature. A similar effect is observed in the He_α line and K_α line emission in Be-like Si; in these cases blending occurs with transitions in Li- and B-like Si, respectively.

K_α line emission has been reported and used for target preheating estimates since the early days of laser-driven fusion experiments and in laser-produced plasmas obtained with CO_2 lasers [20–23] and in target-physics experiments at the particle beam fusion accelerator [24]. However, this time an unusually strong high-order satellite emission is seen in the experimental K_α data. We conjecture that this is due to a combination of high-density and transient effects; this hypothesis is supported by a spectroscopic analysis and numerical modeling.

In Sec. II we discuss the experimental setup and measure-

ments. In Secs. III and IV we discuss the line-shape calculations and present the results of the line broadening analysis of the K_α silicon spectra associated with the Be-, Li-, and He-like ions, including natural, Stark, opacity, and instrumental broadening, and discuss the overall line intensity ratios inferred from the spectroscopic analysis. Finally, in Sec. V we present our conclusions.

II. EXPERIMENTAL SETUP AND RESULTS

The experiments have been carried out using the CPA terawatt titane:sapphire laser system ($\lambda \approx 800$ nm) at the Laboratoire d'Optique Appliquée in Palaiseau. This system is capable of delivering 120-fs duration, 60 mJ of energy, 10-Hz repetition rate pulses at intensities well above 10^{17} W/cm^2. The laser is equipped with a specially designed doublet stretcher [25] to compensate for phase errors of third and fourth order. With this important addition, the laser intensity contrast ratio is measured to be better than 10^{-8} (at 1 ps before the main pulse) by third-order autocorrelation techniques.

The laser polarization and incidence angle in these experiments were chosen to maximize laser absorption under conditions of strong resonance absorption [26–28]. The laser, polarized in the plane of incidence (P polarization), was focused with an $f/16$ fused silica lens on flat silica targets at an angle of 60° with respect to the normal of the target plane [29]. The target was slightly displaced along the laser axis by 2 mm from the ideal focusing position. This provided an elliptical focal spot of 40×80 μm^2 size at $1/e$ of the maximum intensity and a laser irradiance of 10^{16} W/cm^2.

Targets were mounted on an X-Y motorized translational system in order to expose a fresh surface of the target to each laser shot. Time-integrated K_α line emissions were dispersed by a Von Hamos spectrograph built with a curved pentaerythritol ($2d = 8.742$ Å) crystal having a 10 cm radius of curvature. Light intensities were measured with a cooled (-40 °C) x-ray sensitive charge coupled device (CCD) camera operating in the single photon counting mode. It was set at an angle of $30° \pm 3°$ from the normal of the target plane.

Spectra were integrated over a series of 50 shots. Since the registered spectral range was close to the silicon K edge (1840 eV) of the detector material, we had to take into account the relatively high probability of occurrence of partial and pixel-shared events in the analysis of the signal. This was done using pattern recognition techniques that are standard in the astrophysical community [30]. To decrease the background of the CCD image (which was attributed to high-energy electron-induced x-ray fluorescence from the crystal) and thus improve the spectral resolution, we have shielded the entire interaction region (target plus holder) with 1-cm-thick lead foils and we have fitted the entrance port of the spectrograph with a permanent magnet producing a static magnetic field of 500 G parallel to the CCD detector plane.

The size of the CCD matrix being 10×10 mm^2, four successive translations of the camera were necessary to record a complete spectrum. Figure 1(a) shows the spectrum obtained on a flat silicon target for a laser pulse duration of 120 fs. Figure 1(b) shows another spectrum obtained under the same irradiance conditions, but with a laser pulse duration of 2.5 ps. This duration was obtained by slightly detuning the grating pair of the compressor stage. To obtain a similar laser irradiance on target, the target defocusing along the laser axis was reduced to 1 mm and the laser energy was slightly increased. In both spectra, the spectral range covers the photon energy range between 1810 and 1870 eV, which corresponds to the $1s$-$2p$ transitions of the Be-like ion to the He-like Si ion. For the longer pulse duration, the lines are narrower, indicative of an electron density significantly lower than the solid density. The spectrum obtained with a pulse duration of 120 fs is surprisingly different. Satellite lines from Be-like and Li-like ionization stages are more intense than the He-like resonance line and the line shapes are broader. The Li-like satellites around 1840 eV show little structure, but now the low-energy-side peak rises and becomes more intense than the high-energy side of the spectral feature.

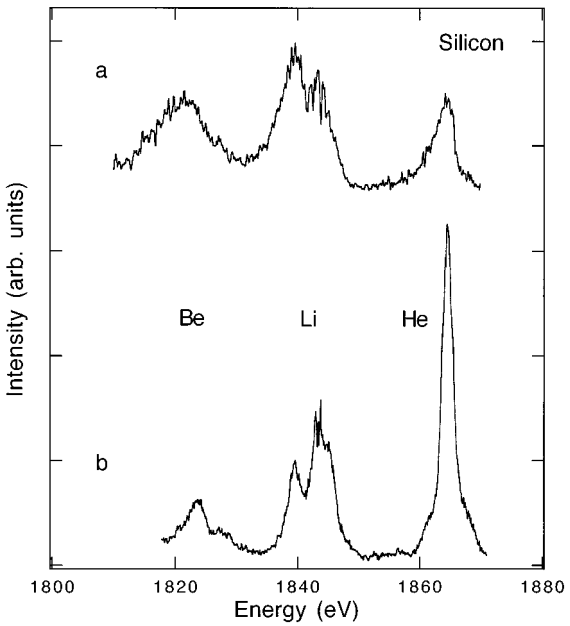

FIG. 1. Experimental silicon spectrum associated with the Be-, Li-, and He-like ions: (a) short pulse (0.12 ps) and (b) long pulse (2.5 ps). The spectra have been shifted vertically by arbitrary amounts for the sake of display in the same figure.

At this stage, the difference between these two spectra can be qualitatively explained by taking into account the strong variations of the electron density gradient scale length with the pulse duration. With the shorter pulse duration, the laser interacts directly with the solid target and we observe a spectrum that is characteristic of a high-density plasma ($N_e \geqslant 10^{23}$ cm^{-3}). We note again that the laser intensity contrast ratio is better than 10^{-8} in these experiments. For longer pulse durations, the electron density gradient scale length increases and the spatial region where He-like and satellite emissions occur is shifted towards lower, but still overcritical (as suggested by the absence of the intercombination line at approximately 1860 eV), electron densities. The long-pulse Li-like satellites and He$_\alpha$ line spectra are similar to those obtained in previous experiments where the laser pulses interacted with an expanding plasma and transient effects were noticeable [10–12]. In the present short-pulse experiments performed at 60° incidence angle the combination of high-contrast pulse and high (resonance) ab-

sorption allows one to observe emission from a denser and cooler plasma.

III. SPECTRAL LINE BROADENING ANALYSIS

Previous calculations of resonance K_α satellite properties for aluminum plasmas have shown that the K_α satellite lines can be classified in two distinct groups [31,32]: one involving ''ordinary'' or low-order satellite transitions of the type $1s2s^r2p^q \rightarrow 1s^22s^r2p^{q-1}$ and the other involving high-order transitions of the type $1s2s^r2p^{q-1}3l \rightarrow 1s^22s^r2p^{q-2}3l$. The former gives the characteristic satellite-line position of an ion; we note that there is a one-to-one correspondence between resonance K_α satellite lines and ionization stages. The latter overlaps mostly with the low-energy wing of the resonance K_α lines of the next-higher ionization stage. This very peculiar feature, which occurs for elements of atomic number Z in the range $10<Z<15$, can give rise to very broad line shapes coming from the contributions of the K_α satellites that are produced by transitions with a high-order n (primarily $n=3$) spectator electron. In this paper we label the spectral features according to the ion that contributes with low-order transitions.

Stark broadened line shapes were calculated for the K_α emission ($2p$-$1s$ line transitions) using a multielectron radiator line profile code that takes into account the effects due to the microfields of the plasma ions and electrons. The effect of the ions was calculated in the static ion approximation, while that of the electrons using a quantum-mechanical second-order, relaxation theory [33,34]. The ion microfield distribution function was computed using the APEX model, extended to consider the case of different ion and electron temperatures [35,36].

Considering the relatively weak He_α line and stronger K_α emission in lower ionization stages observed in the experimental spectrum [see Fig. 1(a)], Stark broadening calculations were done assuming a representative electron temperature $T_e=100$ eV, ion temperatures $T_i=20$ and 100 eV, and electron densities $N_e=1\times10^{23}$, 2×10^{23}, 5×10^{23}, and 1×10^{24} cm^{-3}. During the rapid heating that takes place in laser plasmas produced by subpicosecond pulses, the ion temperature T_i lags behind that of the electrons, thus leading to a situation where ions and electrons have different temperatures; this effect can change the ion microfield distribution function. The two values of T_i considered here result in different ion microfield distribution functions with the higher T_i case ($T_i=T_e=100$ eV), giving more weight to larger microfield values. However, because it was found that for these line transitions and plasma conditions the Stark broadening effect is dominated by the plasma electrons, the changes in the ion microfield distribution function result in a small effect in the final line shape. Electron broadening effects were computed for both upper and lower energy levels of the transitions and the broadening effect on the lower levels was found to be important. Doppler broadening was included, but it is negligible. The upper levels of K_α line transitions in silicon are autoionizing states that can undergo radiative and Auger decays with rates in the order of 10^{13} and 10^{14} s^{-1}, respectively; level widths associated with these rates are less than 0.5 eV. Hence the finite lifetime of the upper levels of these transitions does not contribute significantly to the overall broadening, which, for our cases of interest, is dominated by the Stark effect.

The atomic physics data necessary for the line-shape calculations (i.e., energy levels and electric dipole matrix elements) were obtained using Cowan's atomic structure codes, including relativistic effects [37]. Since the relative position and overlapping between different groups of line transitions is very important in the analysis of the experimental spectra, some of these results were cross-checked for consistency with atomic data calculated using the MZ code. The MZ code uses a $1/Z$ perturbation theory type of approach and also includes relativistic and configurational mixing effects [38]. We considered low-order transitions between energy levels associated with the upper-lower configurations $1s2l$-$1s^2$ in He-like Si, $1s2l2l'$-$1s^22l$ in Li-like Si, and $1s2l2l'2l''$-$1s^22l2l'$ in Be-like Si, where $l,l',l''=s,p$. For example, for Li-like Si the following upper-level configurations were included: $1s2s^2$, $1s2s2p$, and $1s2p^2$, and for the lower level configurations: $1s^22s$ and $1s^22p$; this gives rise to a problem with 16 upper energy levels and 3 lower energy levels. For He-like Si there are 6 upper energy levels and one lower energy level and for Be-like Si there are 30 upper energy levels and 10 lower energy levels.

In addition, spectra from higher-order transitions, i.e., $2p$-$1s$, with one spectator electron in $n=3$ were also computed for B-, Be-, and Li-like Si ions. The presence of the $n=3$ electron in the orbitals considerably increases the number of associated energy levels and thus the complexity of the Stark broadening calculation, which further splits J energy levels according to M sublevels. Even after extensive use of matrix block diagonalization and vectorization techniques [34], the problem is still computationally challenging; to illustrate this point we note that for the B-like ion system (the most complicated case considered here) there are 405 upper- and 110 lower-energy levels associated with the configurations $1s2l2l'2l''3l'''$ and $1s^22l2l'3l'''$, where $l,l',l''=s,p$ and $l'''=s,p,d$. Hence, in some of these calculations only a subset of the relevant set of configurations were included in the line-shape calculations. The decision was based on practical considerations (i.e., computer time and memory) and on the idea of trying to use in each case the set of transitions that made the largest contribution to the spectra. For Li-like Si it was possible to include all relevant configurations, namely, $1s2s3s$,$1s2p3s$,$1s2s3p$,$1s2p3p$, $1s2s3d$,$1s2p3d$,$1s^23s$,$1s^23p$, and $1s^23d$; this set of configurations gives rise to 66 upper and 5 lower energy levels. For Be-like Si the following configurations were included: $1s2p^23s$,$1s2p^23p$,$1s2p^23d$,$1s^22p3s$,$1s^22p3p$, and $1s^22p3d$; this set of configurations gives rise to 114 upper and 26 lower energy levels. B-like Si presents the most complicated case and no $3d$ spectator electron was included. The configurations considered were $1s2s2p^23s$,$1s2s2p^23p$, $1s2p^33s$,$1s2p^33p$,$1s^22s2p3s$,$1s^22s2p3p$,$1s^22p^23s$, and $1s^22p^23p$; this set of configurations gives rise to a problem with 178 upper and 54 lower energy levels.

The subset of configurations considered for high-order transitions in B- and Be-like Si can also affect the result of the Stark broadening calculation since the associated energy levels control field mixing effects within the sets of upper and lower energy levels. To check this point, line-shape cal-

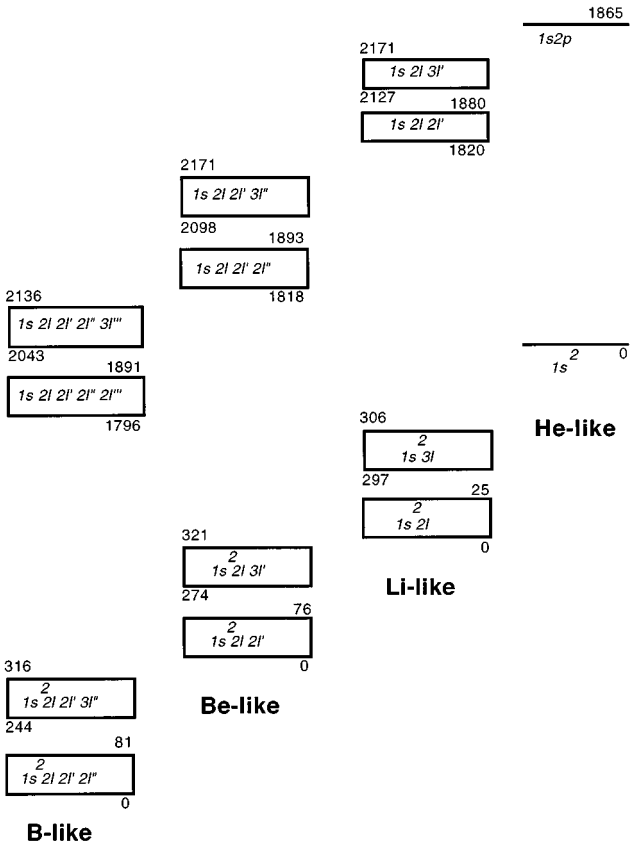

FIG. 2. Schematic Grotrian diagram of the relevant ionization stages and groups of energy levels. Each box represents a group of energy levels associated with a set of configurations where $2l,2l',2l'',2l'''$ can be $2s$ or $2p$ and $3l,3l',3l'',3l'''$ can be $3s$, $3p$, or $3d$; also indicated are lower and upper energy bounds in eV for the group of levels in each box counted from the ground state of each ion. The average energy differences between the ground configurations of B-, Be-, Li-, and He-like Si ions are 397, 476, and 523 eV, respectively.

culations were done including different combinations of subsets of configurations; based on this, we estimate uncertainties in the line shape due to this approximation to be less than 12%.

Figure 2 displays a schematic Grotrian diagram of the relevant ionization stages and energy levels. Because of the reduced screening effect of the $n=3$ spectator electron of the high-order transitions, these transitions shift towards larger energies and overlap with low-order transitions in the next higher ionization stage. The overlapping between resonance K-shell lines and higher-order satellites in He- and Li-like ions, and also in the general context of K_α lines in L-shell ions and their higher-order satellite lines, is important in the proper analysis and interpretation of these spectral features; its relevance has been pointed out for astrophysical plasmas [39], proton-driven plasmas [31,32], laser-driven fusion plasmas [40,41], picosecond-pulse laser-produced plasmas [42], and even opacity modeling [43,44]. However, in the experimental results shown in this paper this effect is unusually strong. To illustrate this point, Fig. 3 displays the short-pulse experimental spectrum and the details of the theoretical spectra associated with each spectral feature. For instance, for the Li-like feature the overlapping between low-order Li and high-order Be (Be*) transitions is significant and the blending of these two emissions gives rise to a composite spectral feature. In particular, the high-order Be emission contribution dominates the low-energy side of the spectral feature. Similarly, there is overlapping between B high-order and Be low-order transitions (B*/Be) and between Li high-order and He low-order transitions (Li*/He). Partially shown in the experimental spectrum in Fig. 3 (also in Figs. 4 and 5) is the B-like K_α spectral feature (1800 eV).

For the electron densities N_e considered here the Stark broadening effect dominates the line profile and introduces density sensitivity in the line shapes of both low- and high-order transitions, which can be used to infer the average plasma electron densities at which the spectrum was emitted. This sensitivity is even more pronounced for the case of high-order transitions since the orbitals with an $n=3$ electron are less tightly bound and hence easier to perturb by the plasma microfields. Thus the overlapping and blending of Stark broadened K_α lines associated with low- and high-order transitions in adjacent ionization stages generates a composite spectral feature whose overall shape and broadening are density dependent.

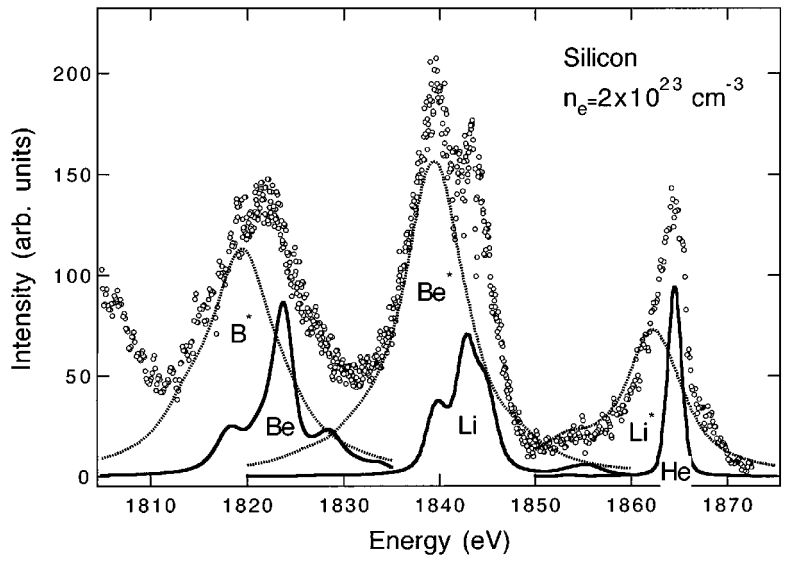

FIG. 3. Experimental short-pulse silicon spectrum (○) and detail of the theoretical spectrum at $N_e=2\times10^{23}$ cm^{-3} for Be-, Li-, and He-like Si showing the individual contributions due to low-order (—) and high-order (– –) transitions. Partially shown in the experimental spectrum (low-energy end) is the B-like Si K_α spectral feature.

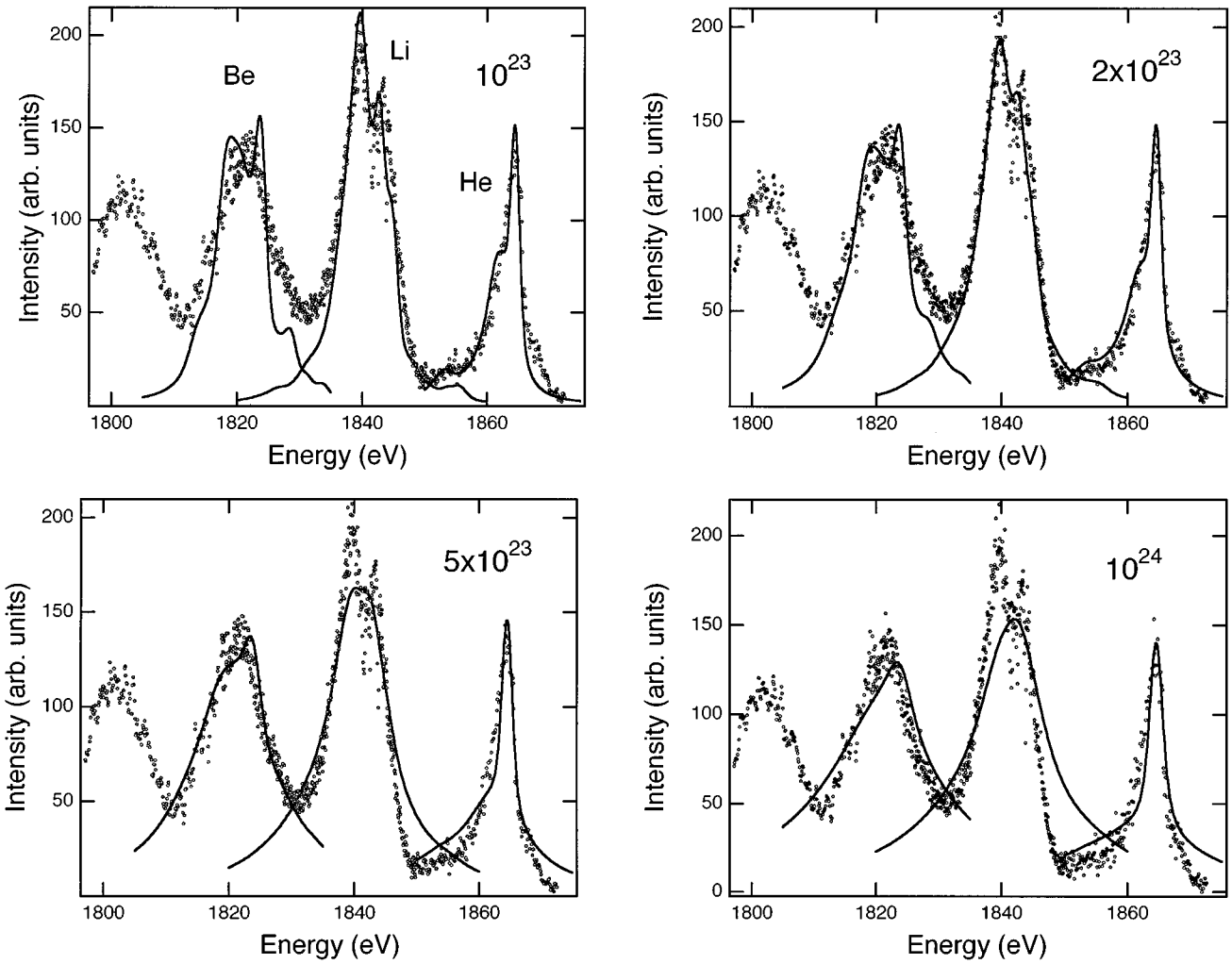

FIG. 4. Comparison of the Stark-broadened theoretical (—) and experimental short-pulse spectra (○) for the Be-, Li-, and He-like Si ions for electron densities $N_e = 1\times10^{23}$, 2×10^{23}, 5×10^{23}, and 1×10^{24} cm^{-3}. Each spectral feature includes low-order transitions in a given ion and high-order transitions in the next, lower ionization stage. Partially shown in the experimental spectra is the B-like Si K_α spectral feature (1800 eV).

In Fig. 4 we display the comparison between experimental and synthetic spectra for the Be, Li, and He spectral features, for several electron densities N_e. The theoretical spectra also includes instrumental broadening effects. In each spectral feature the relative adjustment of total intensities between low- and high-order transitions has been selected in order to produce the best comparison with the experiment using a least-squares minimization procedure. In turn, this procedure gives the ratio of total intensities of low- and high-order K_α line transitions responsible for each composite spectral feature. Figure 5 shows theoretical fits to the experimental spectrum for the two electron densities that produce the best simultaneous fit to the Be, Li, and He spectral features. From these results it appears that the experimental spectrum is characteristic of electron densities N_e in the range from 1×10^{23} to 2×10^{23} cm^{-3}, i.e., comparable to the silicon solid density. Since this spectrum is time and spatially integrated, these electron densities have to be interpreted as average or effective. Most likely, the spectra was built gradually with different ions making their contribution at slightly different times. In this connection, it is interesting to note that the Be spectral feature seems to be characteristic

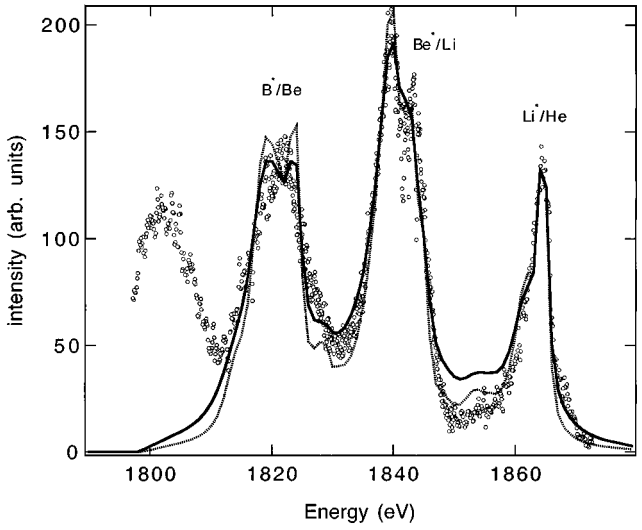

FIG. 5. Comparison of the experimental short pulse (○) and composite theoretical silicon spectra at $N_e = 1\times10^{23}$ cm^{-3} (– –) and 2×10^{23} cm^{-3} (—). Partially shown in the experimental spectrum is the B-like Si K_α spectral feature (1800 eV).

TABLE I. Calculated effective ionization ($T_{\rm ion}$) and excitation ($T_{\rm exc}$) temperatures of a silicon plasma produced by a 120-fs laser pulse at 10^{16} W/cm^2.

Satellite feature	Intensity ratio	$T_{\rm exc}$ (eV)	$T_{\rm ion}$ (eV)
I(B*)/I(Be)	2.8		80 ± 5
I(Be*)/I(Li)	3.9		85 ± 5
I(Li*)/I(He)	4.1		92 ± 5
I(Be*)/I(Be)	2.6	315 ± 40	
I(Li*)/I(Li)	1.3	390 ± 40	

of densities higher than the Li and He features. This is consistent with the picture that emission from lower ionization stages comes from deeper regions of the target that will undergo less decompression as compared to the front regions of the target and thus they can produce spectra characteristic of higher densities.

Opacity broadening could also be responsible for part of the overall broadening in which case electron densities deduced from the Stark line broadening analysis would be lower. However, the optical depth τ_ν for these lines is estimated to be less than 0.1; hence opacity broadening makes a small contribution.

Another interesting feature of the analysis is the strong contribution from high-order transitions. From Figs. 3 and 4, for the case of the Li spectral feature, it is clear that the broad peak in the low-energy side of the spectral feature is dominated by higher-order transitions in Be-like Si. This effect is also seen in the He and Be spectral features. In fact, the ratios of total intensities of high-order emission to low-order emission deduced from the line broadening analysis are in the range 2.8–4.1 (see Table I), indicating that this spectrum was formed under conditions where there was an overpopulation of $n=3$ energy levels. A comparison (see Fig. 1) between the short- and long-pulse spectra suggests that in the short-pulse experiment a combination of high-density and time-dependent effects led to a transient overpopulation of the upper levels of $n=3$ energy levels that resulted in an unusually strong emission of high-order transitions.

The question arises as to whether or not emission from $n=4$ energy levels can be important. Population in $n=4$ levels can also be enhanced and this can lead to significant emission from these energy levels; however, emission from these levels (and higher n levels) will be further broadened by the plasma microfields and will overlap even more with the low-order K_α of the next higher ionization stage, eventually contributing to build a ''pedestal'' for the low-order emission. Unfolding this effect from the spectra would require detailed atomic kinetics modeling in conjunction with line-shape calculations and it is beyond the scope of this paper.

IV. LINE INTENSITY ANALYSIS

For the electron temperature and density conditions of our experiments ($T_e\approx100$ eV and $N_e\approx10^{23}$ cm^{-3}) we have shown in Sec. III that the Stark effect can be significant to broaden the K_α satellite lines, particularly from excited configurations with M-shell spectator electrons. Due to the expense of fully time-dependent hydrodynamics coupled to atomic physics and line-shape calculations, it was not feasible to do a truly comprehensive set of runs closely covering all the expected conditions encountered in our experiments. Nevertheless, essential conclusions can be drawn for much of the important physics of K_α resonance satellite production by using the concept of the effective ionization and excitation temperatures [45]. These quantities can be determined by using Boltzmann (excitation temperature) and Saha (ionization temperature) statistics among each single ion and its next higher charge neighbor. We performed calculations for atomic energy levels and radiative transition probabilities using, for convenience, the HULLAC atomic physics package of computer programs [46–48]. Results were also cross-checked for consistency with Cowan's code results. The frequency averaged intensities of the K_α resonance satellite transitions can be estimated by

$$I=\int I(\nu)d\nu=N_u h\nu A_{ul},$$

where N_u is the excited configuration population and A_{ul} the effective radiative rate. The effective rates between the configurations described in Sec. III for the B-, Be-, Li-, and He-like ions were calculated by averaging the sum of the individual level transition rates calculated by HULLAC. Then, the ratio I_1/I_2 of two satellite intensities is simply estimated by using

$$\frac{I_1}{I_2}=\frac{N_u^1 h\nu^1 A_{ul}^1}{N_u^2 h\nu^2 A_{ul}^2},$$

where N_u^1/N_u^2 is calculated assuming LTE conditions with a Boltzmann or a Saha population ratio factor for lines originating from the same ion or from two adjacent ions, respectively. Knowing the statistical weights, the comparison of the experimental and calculated intensity ratios gives an effective excitation temperature for two satellite features originating from the same ion and an effective ionization temperature for two satellite features originating from two adjacent ions. We assume an electron density in the range $(1-2)\times10^{23}$ cm^{-3} deduced from the Stark broadening analysis of Sec. III.

This crude analysis is meaningful only if the reabsorption effects (photon escape probability and line broadening) are negligible. A recent analysis performed for aluminum plasmas [49], scaled to our case of silicon, shows that the effects can be reasonably assumed to be small under our low laser prepulse intensity conditions due to the rather small optical depth ($\tau_\nu<0.1$) of our plasma. Table I gives a summary of the results. Intensity ratios inferred from the experiment were obtained doing the line broadening analysis discussed in Sec. III.

Two important conclusions can be drawn from this simple analysis. First, results of effective excitation and ionization temperatures show very consistent values when one goes from the B-like to the He-like ion. The excitation temperature shows more dispersion because the intensity ratio of line features originating from configurations with a $n=3$ and $n=2$ spectator electron is only slightly dependent on temperature for temperatures larger than the energy gap between their respective upper configurations. Second, the low effec-

tive ionization temperature points to the fact that most of the time-integrated emission that we measure originates from the target bulk in density regions (close to solid density) where the electron heating is predominantly ruled by thermal conduction [4,8]. The large difference between the excitation and ionization temperature is more surprising. Non-steady-state population kinetics probably play an important role [8] in overpopulating the M-shell spectator electron configurations. This can be due to the effect of hot electrons, i.e., nonthermal electrons that arise from resonance absorption at the high angle of incidence that we have used in the experiments. Specific collisional-radiative population rates should be introduced to perform a fully time-dependent calculation of population kinetics taking into account the exact shape of the electron energy distribution function [50], as well as inner-shell ionization and excitation processes of energy levels with an $n=3$ spectator electron. Inner-shell ionization and excitation driven by hot electrons have already shown to play an important role in the detailed modeling of population kinetics of Li-like $1s2l2l'$ levels in transient aluminum plasmas [12].

V. CONCLUSIONS

We have reported in this paper an experimental study and line broadening analysis of x-ray line emission from silicon targets irradiated at large incidence angle (60°) with ultrashort (120 fs) P-polarized laser pulses at high intensities ($\approx 10^{16}$ W cm^{-2}) and a high-intensity contrast ratio (10^{-8}). Silicon K_α emission shows two main characteristics: significant broadening dominated by the Stark effect due to the plasma microfields and a strong contribution from higher-order satellite transitions. The relevance of the Stark broadening effect is indicative of the average, high densities of which this emission is characteristic. The high-order K_α emission also contributes to the overall broadening of each spectral feature.

Stark broadened line shapes were calculated for the K_α emission using a multielectron radiator line profile code that takes into account the effects due to the microfields of the plasma ions and electrons. From the results it appears that the experimental spectrum is characteristic of electron densities N_e in the range from 1×10^{23} to 2×10^{23} cm^{-3}, i.e., comparable to the silicon solid density. Since this spectrum is time and spatially integrated these electron densities have to be interpreted as average quantities.

The ratios of total intensities of high-order emission to low-order emission deduced from the line broadening analysis are in the range 2.8–4.1, indicating that this spectrum was formed under conditions where there was an overpopulation of $n=3$ energy levels. High-density and time-dependent effects can, in principle, contribute to the amount of high-order satellite emission present in these spectra, and both are consistent with the experimental conditions. However, it is not clear at present if one of these two effects played a dominant role.

ACKNOWLEDGMENTS

We wish to acknowledge the very generous help of M. Klapisch in the use of the HULLAC computer code. This work was supported by the Centre National de la Recherche Scientifique, EEC Grant No. ERBCHRXCT930346 of the ''Human Capital and Mobility'' program, and by NSF Grant Nos. OSR-9353227 and INT-9416720.

[1] H.M. Milchberg, R.R. Freeman, S.C. Davey, and R.M. More, Phys. Rev. Lett. **61**, 2364 (1988).
[2] M.M. Murnane, H.C. Kapteyn, and R.W. Falcone, Phys. Rev. Lett. **62**, 155 (1989).
[3] J.C. Kieffer, M. Chaker, J.P. Matte, H. Pepin, C.Y. Coté, Y. Beaudoin, T.W. Johnston, C.Y. Chien, S. Coe, and G. Morou, Phys. Fluids B **5**, 2676 (1993).
[4] H.M. Milchberg, I. Lyubomirsky, and C.G. Durfee III, Phys. Rev. Lett. **67**, 2564 (1991).
[5] P. Audebert, J.P. Geindre, J.C. Gauthier, A. Mysyrowicz, J.P. Chambaret, and A. Antonetti, Europhys. Lett. **19**, 189 (1992).
[6] U. Teubner, C. Wulker, W. Theobald, and E. Förster, Phys. Plasmas **2**, 972 (1995).
[7] Z. Jiang, J.C. Kieffer, J.P. Matte, M. Chaker, O. Peyrusse, D. Giles, G. Korn, A. Maksimchuk, S. Coe, and G. Mourou, Phys. Plasmas **2**, 1702 (1995).
[8] P. Audebert, J.P. Geindre, A. Rousse, F. Falliès, J.C. Gauthier, A. Mysyrowicz, G. Grillon, and A. Antonetti, J. Phys. B **27**, 3303 (1994).
[9] J. Davis, R. Clark, and J. Giuliani, Laser Part. Beams **13**, 3 (1995).
[10] O. Peyrusse, J.C. Kieffer, C.Y. Coté, and M. Chaker, J. Phys. B **26**, L511 (1993).
[11] J.P. Matte, J.C. Kieffer, S. Ethier, M. Chaker, and O. Peyrusse, Phys. Rev. Lett. **72**, 1208 (1994).
[12] R.C. Mancini, P. Audebert, J.P. Geindre, A. Rousse, F. Falliès, J.C. Gauthier, A. Mysyrowicz, J.P. Chambaret, and A. Antonetti, J. Phys. B **27**, 1671 (1994).
[13] H. Chen, B. Soom, B. Yaakobi, S. Uchida, and D.D. Meyerhofer, Phys. Rev. Lett. **70**, 3431 (1993).
[14] B. Soom, H. Chen, Y. Fisher, and D.D. Meyerhofer, J. Appl. Phys. **74**, 5372 (1993).
[15] A. Rousse, P. Audebert, J.P. Geindre, F. Falliès, J.C. Gauthier, A. Mysyrowicz, G. Grillon, and A. Antonetti, Phys. Rev. E **50**, 2200 (1994).
[16] J.C. Gauthier, J.P. Geindre, P. Audebert, A. Rousse, A. Dos Santos, G. Grillon, A. Antonetti, and R.C. Mancini, Phys. Rev. E **52**, 2963 (1995).
[17] O. Peyrusse, M. Busquet, J.C. Kieffer, Z. Jiang, and C.Y. Coté, Phys. Rev. Lett. **75**, 3862 (1995).
[18] V.L. Jacobs, J.E. Rogerson, M.H. Chen, and R.D. Cowan, Phys. Rev. A **32**, 3382 (1985), and references therein.
[19] L.A. Woltz, V.L. Jacobs, C.F. Hooper, Jr., and R.C. Mancini, Phys. Rev. A **44**, 1281 (1991).
[20] B. Yaakobi, I. Pelah, and J. Hoose, Phys. Rev. Lett. **37**, 836 (1976).

[21] J. Hares, J.D. Kilkenny, M.H. Key, and J.G. Lunney, Phys. Rev. Lett. **42**, 1216 (1979).
[22] A. Hauer, W. Priedhorsky, and D. van Hulsteyn, Appl. Opt. **20**, 3477 (1981).
[23] N.H. Burnett, G.D. Enright, A. Avery, A. Loen, and J.C. Kieffer, Phys. Rev. A **29**, 2294 (1984).
[24] J. Bailey, A.L. Carlson, G. Chandler, M.S. Derzon, R.J. Dukart, B.A. Hammel, D.J. Johnson, T.R. Lockner, J. Maenchen, E.J. McGuire, T.A. Mehlhorn, W.E. Nelson, L.E. Ruggles, W.A. Stygar, and D.F. Wenger, Laser Part. Beams **8**, 555 (1990).
[25] A. Sullivan and W.E. White, Opt. Lett. **20**, 192 (1995).
[26] R. Fedosejevs, R. Ottmann, R. Sigel, G. Kühnle, S. Szatmari, and F.P. Schäfer, Appl. Phys. B **50**, 79 (1990).
[27] R. Fedosejevs, R. Ottmann, R. Sigel, G. Kühnle, S. Szatmari, and F.P. Schäfer, Phys. Rev. Lett. **64**, 1250 (1990).
[28] U. Teubner, J. Bergmann, B. van Wonterghem, F.P. Schäfer, and R. Sauerbrey, Phys. Rev. Lett. **70**, 794 (1993).
[29] J.C. Gauthier, S. Bastiani, P. Audebert, J.P. Geindre, K. Neuman, T. Donnelly, M. Hoffer, R.W. Falcone, R. Shepherd, D. Price, and B. White, SPIE Proc. **2523**, 242 (1995).
[30] C. Pigot, M. Lortholary, and P. Mulet (private communication).
[31] J.J. MacFarlane, P. Wang, J. Bailey, T.A. Mehlhorn, R.J. Dukart, and R.C. Mancini, Phys. Rev. E **47**, 2748 (1993).
[32] P. Wang, J.J. MacFarlane, and G.A. Moses, Phys. Rev. E **48**, 3934 (1993).
[33] L.A. Woltz and C.F. Hooper, Jr., Phys. Rev. A **38**, 4766 (1988).
[34] R.C. Mancini, D.P. Kilcrease, L.A. Woltz, and C.F. Hooper, Jr., Comput. Phys. Commun. **63**, 314 (1991).
[35] C.A. Iglesias, H.E. DeWitt, J.L. Lebowitz, D. Mac Gowan, and W.B. Hubbard, Phys. Rev. A **31**, 1698 (1985).
[36] D.P. Kilcrease, J. Quant. Spectrosc. Radiat. Transfer **51**, 161 (1994).
[37] R.D. Cowan, *The Theory of Atomic Structure and Spectra* (University of California Press, Berkeley, 1981).
[38] U.I. Safronova, Phys. Scr. **T26**, 59 (1989).
[39] F. Bely-Dubau, J. Dubau, P. Faucher, and A.H. Gabriel, Mon. Not. R. Astron. Soc. **198**, 239 (1982), and references therein.
[40] R.C. Mancini, C.F. Hooper, Jr., N.D. Delamater, A. Hauer, C.J. Keane, B.A. Hammel, and J.K. Nash, Rev. Sci. Instrum. **63**, 5119 (1992).
[41] C.J. Keane, B.A. Hammel, D.R. Kania, J.D. Kilkenny, R.W. Lee, A.L. Osterheld, R.C. Mancini, C.F. Hooper, Jr., and N.D. Delamater, Phys. Fluids B **5**, 3328 (1993).
[42] F.B. Rosmej, B.A. Bryunetkin, A. Ya Faenov, Yu Skobelev, M.P. Kalashnikov, P.V. Nickles, and M. Schnürer, J. Phys. B **29**, L299 (1996).
[43] J. Abdallah, Jr., R.E.H. Clark, and J.M. Peek, Phys. Rev. A **44**, 4072 (1991).
[44] R.C. Mancini, C.F. Hooper, Jr., and R.L. Coldwell, J. Quant. Spectrosc. Radiat. Transfer **51**, 201 (1994).
[45] M. Busquet, in *Radiative Properties of Hot Dense Matter*, edited by W. Goldstein, C.F. Hooper, Jr., J.C. Gauthier, J. Seely, and R.W. Lee (World Scientific, Singapore, 1991), p. 332.
[46] M. Klapisch, J.L. Schwob, B.S. Fraenkel, and J. Oreg, J. Opt. Soc. Am. **67**, 148 (1977).
[47] A. Bar-Shalom, M. Klapisch, and J. Oreg, Phys. Rev. A **38**, 1773 (1988).
[48] A. Bar-Shalom and M. Klapisch, Comput. Phys. Commun. **50**, 375 (1988).
[49] J.P. Apruzese, Phys. Rev. E **47**, 2798 (1993).
[50] Y.T. Lee and M. Lamoureux, Phys. Fluids B **5**, 2235 (1993).